Journal of Zhejiang University-SCIENCE A (Applied Physics & Engineering)
ISSN 1673-565X (Print); ISSN 1862-1775 (Online)
www.jzus.zju.edu.cn; link.springer.com
E-mail: jzus_a@zju.edu.cn

Compressive behavior of hybrid steel-polyvinyl alcohol fiber-reinforced concrete containing fly ash and slag powder: experiments and an artificial neural network model*#

Fang-yu LIU[1], Wen-qi DING[2,3], Ya-fei QIAO[†‡2,3], Lin-bing WANG[†‡1], Qi-yang CHEN[4]

[1]*Department of Civil and Environmental Engineering, Virginia Polytechnic Institute and State University, Virginia 24061, USA*

[2]*Department of Geotechnical Engineering, College of Civil Engineering, Tongji University, Shanghai 200092, China*

[3]*Key Laboratory of Geotechnical and Underground Engineering, Ministry of Education, Shanghai 200092, China*

[4]*Department of Civil and Environmental Engineering, University of Illinois at Urbana-Champaign, Urbana 61801, USA*

[†]E-mail: yafei.qiao@tongji.edu.cn; wangl@vt.edu

Received Aug. 23, 2020; Revision accepted Nov. 11, 2020; Crosschecked Sept. 3, 2021

Abstract: Understanding the mechanical behavior of hybrid fiber-reinforced concrete (HFRC), a composite material, is crucial for the design of HFRC and HFRC structures. In this study, a series of compression experiments were performed on hybrid steel-polyvinyl alcohol (PVA) fiber-reinforced concrete containing fly ash and slag powder, with a focus on the fiber content/ratio effect on its compressive behavior; a new approach was built to model the compression behavior of HFRC by using an artificial neural network (ANN) method. The proposed ANN model incorporated two new developments: the prediction of the compressive stress-strain curve and consideration of 23 features of components of HFRC. To build a database for the ANN model, relevant published data were also collected. Three indices were used to train and evaluate the ANN model. To highlight the performance of the ANN model, it was compared with a traditional equation-based model. The results revealed that the relative errors of the predicted compressive strength and strain corresponding to compressive strength of the ANN model were close to 0, while the corresponding values from the equation-based model were higher. Therefore, the ANN model is better able to consider the effect of different components on the compressive behavior of HFRC in terms of compressive strength, the strain corresponding to compressive strength, and the compressive stress-strain curve. Such an ANN model could also be a good tool to predict the mechanical behavior of other composite materials.

Key words: Experiments; Artificial neural network (ANN); Hybrid fiber-reinforced concrete (HFRC); Compressive behavior; Stress-strain curve

https://doi.org/10.1631/jzus.A2000379 **CLC number:** TU528.572

1 Introduction

Fiber-reinforced concrete (FRC), a typical composite material, has been successfully and widely used in civil infrastructure, such as tunnels (de la Fuente et al., 2012; Liao et al., 2015; Gong et al., 2017), bridges (Stoll et al., 2000), concrete structures (Sim et al., 2005), and pavements (Belletti et al., 2008). This is because FRC greatly improves tensile behavior (Xu et al., 2011), flexural behavior (Nguyen et al., 2013), and durability (Liu et al., 2019a) compared with concrete. The compression behavior and basic mechanical characteristics of concrete can also be significantly affected by the addition of fibers (Zhou et al., 2018, 2019). Such enhanced compression behavior is important for many concrete

‡ Corresponding author

* Project supported by the National Natural Science Foundation of China (Nos. 51978515 and 52090083), the Shanghai Sailing Program (No. 19YF1451400), and the Shanghai Municipal Science and Technology Major Project (No. 2017SHZDZX02), China

Electronic supplementary materials: The online version of this article (https://doi.org/10.1631/jzus.A2000379) contains supplementary materials, which are available to authorized users

ORCID: Ya-fei QIAO, https://orcid.org/0000-0001-7567-3988

structures, especially in the joints of precast structures where stress is concentrated (Ding et al., 2020). To design a suitable FRC, different types of fibers can be used, including steel, polyvinyl alcohol (PVA), polypropylene (PP), basalt, and synthetic fibers (Sim et al., 2005; Soutsos et al., 2012; Liu et al., 2019a, 2020a). The mechanical behavior of FRC is related to the type of fiber, the geometry of fiber, and the total fiber content (Lawler et al., 2003, 2005; Liu et al., 2020b).

According to the number of fiber types combined, FRC can be categorized as single fiber-reinforced concrete or hybrid fiber-reinforced concrete (HFRC), which includes two or more types of fibers. HFRC generally has better mechanical properties than single fiber-reinforced concrete. This is because the hybridization of different fibers can maximize their contribution to the improvement in the mechanical properties of the concrete mixture (Lawler et al., 2005). These improvements are strongly dependent on the fiber type, fiber volume content, hybrid ratio, fiber aspect ratio, and mechanical properties of the fibers (Lawler et al., 2003, 2005; Blanco et al., 2016; Liu et al., 2019b; Zhou et al., 2019). For instance, steel fibers, a type of macrofiber, could create a bridge effect to prevent the development of a major crack because of their greater length, leading to improvements in tensile strength, crack resistance, toughness, and flexural post-cracking creep behavior (Zhao et al., 2015; Serna Ros et al., 2016; Pujadas et al., 2017; Liu et al., 2020b); PVA fibers, a type of microfiber, could introduce many noticeable microcracks and delay the propagation of macrocracks, thereby improving the toughness of concrete (Lawler et al., 2005; Pujadas et al., 2014; Liu et al., 2019b). Therefore, understanding the effects of these fiber features is important for the design and modeling of HFRC.

To describe the compression behavior of HFRC, many researchers have built models based on the constitutive models of plain concrete (Chi et al., 2014a, 2014b; Zhou et al., 2019). The effects of many features of fibers, such as their length, diameter, and volume, can be introduced into constitutive models via statistical analysis. However, as HFRC exhibits complex responses in terms of strain-softening/hardening, volumetric dilatancy, and pressure sensitivity, these constitutive models are difficult to develop from a purely mathematical perspective (Chi et al., 2014a). They also have limitations for describing the complex compressive behavior of HFRC, especially in capturing the effects of different components.

To overcome these limitations, deep learning methods have recently been applied to predicting the mechanical properties of concrete (Mashhadban et al., 2016) and designing the mix compositions of civil materials (Açikgenç et al., 2015). Artificial neural network (ANN), as one of the basic deep learning methods, has shown its strong application ability in civil engineering. It can be used to analyze the relationship between different types of data, produce a correct or nearly correct response to a large database, and make a good prediction for new data. The ANN method has been successfully used to model the compressive, tensile, and flexural strengths of FRC (Karahan et al., 2008; Mashhadban et al., 2016), predict the mix composition of steel fiber-reinforced concrete (Açikgenç et al., 2015), describe the stress-strain model for fiber reinforced polymer (FRP)-confined concrete (Jiang et al., 2020), and predict the workability of concrete incorporating metakaolin and fly ash (Bai et al., 2003). Since more factors can be considered in an ANN model, it can make more accurate predictions. Moreover, an ANN model is implicit and does not need an experimental data-based formula. However, all the above studies focused on the key characteristics of the mechanical behavior of FRC. Few studies have been carried out to predict the whole stress-strain curve of HFRC using the ANN method. The authors have developed an ANN model to capture the tensile stress-strain relationship of HFRC (Liu et al., 2020a) and attempted to extend it to describe the compressive behavior in this work.

In summary, the compression behavior of HFRC, especially the stress-strain relationship, is important for many types of concrete structures and their modeling. Conventional constitutive models have limitations in describing such complex compression behaviors. Therefore, this study aimed to reveal the compressive behavior of HFRC containing fly ash and slag powder and develop a new approach to model its compressive stress-strain curve by using the ANN method, and to highlight the capability of the ANN model by investigating the effect of different HFRC components on the compressive behavior of HFRC. To accurately represent the effect of different

components of HFRC, the proposed ANN model was used to consider many important factors, including the fiber characteristics (volume, weight, length, diameter, aspect ratio, and reinforcement index), the mechanical properties of plain concrete (elastic modulus, compressive strength, and strain corresponding to compressive strength), and the composition of the concrete mixture (water binder ratio, cement, fly ash, slag powder, water, coarse aggregate, and fine aggregate).

In the following sections, a series of compression tests on HFRC containing fly ash and slag powder were first introduced to reveal its compressive behavior. Then relevant published data were collected to extend the size and diversity of the database. After that, the ANN model was built and trained based on the database and an equation-based model was also proposed. Finally, a comparison between these two models was carried out via the description of the experimental data, followed by the sensitivity analysis of ANN model.

2 Compressive experiments

2.1 Materials

The selected cement was Class 42.5R ordinary Portland cement, which had a specific surface area of 368 m^2/kg. The specific surface area of fly ash was 242 m^2/kg compared with 436 m^2/kg for slag powder. The fly ash had a SiO_2 mass fraction of 54.2% compared with 36.9% for the slag powder. The maximum particle size of the fine aggregate was 5 mm, and the coarse aggregate had a continuous size of 5–20 mm. Other properties of the cement, fly ash, and slag powder can be found in (Liu et al., 2019a). The mass proportions of the concrete mixture were cement:fly ash:slag powder:fine aggregate:coarse aggregate: water:superplasticizer=225:75:75:785:1024:165:3.2, and the water-to-binder ratio was set to 0.44. These were designed according to the Chinese Codes (CAECS, 2010; MHURD, 2011a, 2011b).

As a component of HFRC, fibers significantly affect its mechanical properties, which warrant detailed investigation. In this study, steel fiber and PVA fiber were used, and the detailed properties of these two fibers can be found in (Liu et al., 2019a). To highlight the effects of hybridization and fiber content on the compressive behavior of HFRC, various volume-based hybrid ratios of steel fiber to PVA fiber, ranging from 1:3 to 3:1, were tested, and the total fiber volume content ranged from 1% to 3%. Steel and PVA fiber combinations with fiber volume contents of 0.5%, 1.0%, and 1.5% were tested, based on published values shown to improve the mechanical properties of HFRC (Hai et al., 2016; Feng et al., 2018; Liu et al., 2019b, 2020b). Concrete reinforced with either steel or PVA fiber alone was also tested simultaneously, as well as plain concrete, collectively acting as the control group. Therefore, there are 12 groups of specimens in total and they are named as S_aP_b, where a means the volume content of steel fibers and b means the volume content of PVA fibers. For example, $S_{1.0}P_{1.5}$ means the specimen that consists of 1.0% steel fibers and 1.5% PVA fibers. C means the plain concrete.

2.2 Specimen and experiment program

All concrete specimens were mixed according to the literature, to ensure the uniform dispersion of the fibers (CAECS, 2010; MHURD, 2011a; Li and Liu, 2016; Liu et al., 2019b, 2020b). During mixing of the HFRC samples, more steel fibers had little effect on the workability of HFRC, but increasing the PVA fibers could worsen the workability due to their high-water absorption properties when the proportions of the concrete mix remained constant, as observed in other studies (Hossain et al., 2013; Tabatabaeian et al., 2017). The geometry of the specimen was 150 mm×150 mm×300 mm. A high stiffness testing machine (Fig. 1) with a capacity of 3000 kN was used to carry out the compressive tests. To obtain a better descent part of the compressive stress-strain curve, the test was controlled by a displacement control, loading at a rate of 0.1 mm/min before reaching the peak value, and at a rate of 0.06 mm/min during the post-peak stage. The loading force was recorded by a force sensor. The strain in the middle part of the specimen was measured by an extensometer (Fig. 1) with a gauge length of 100 mm, attached to the side of the specimen.

2.3 Experimental results

Fig. 2 presents typical measured compressive stress-strain curves. The compressive stress increased quickly and almost linearly before reaching the compressive strength at a strain of about 0.002. The

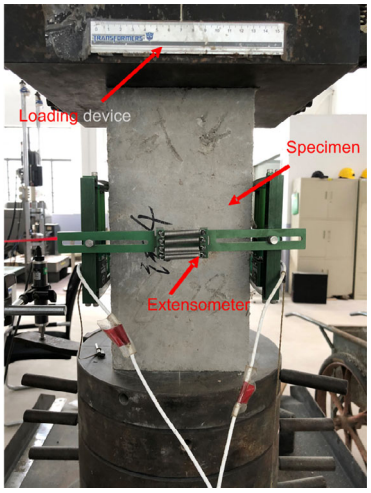

Fig. 1 Compressive test instrument and sensors

compressive stress then dropped nonlinearly as the strain increased. According to Figs. 2a–2c, the peak value of the curve increased as the content of steel fibers increased, but it appeared to decrease when the volume of steel fibers was too high. In comparison, with an increase in PVA fibers, the peak value reduced slightly, and the gap between the different curves widened during the post-peak stage.

Table 1 summarizes the average compressive strength and its corresponding strain for all test specimens. The compressive strength and strain corresponding to compressive strength (SCCS) depended on the fiber volume and the hybrid ratio. The single fiber-reinforced concrete ($S_{1.0}$, $P_{1.0}$) had a higher compressive strength than the plain concrete (C). For the same fiber volume of 1.0%, the

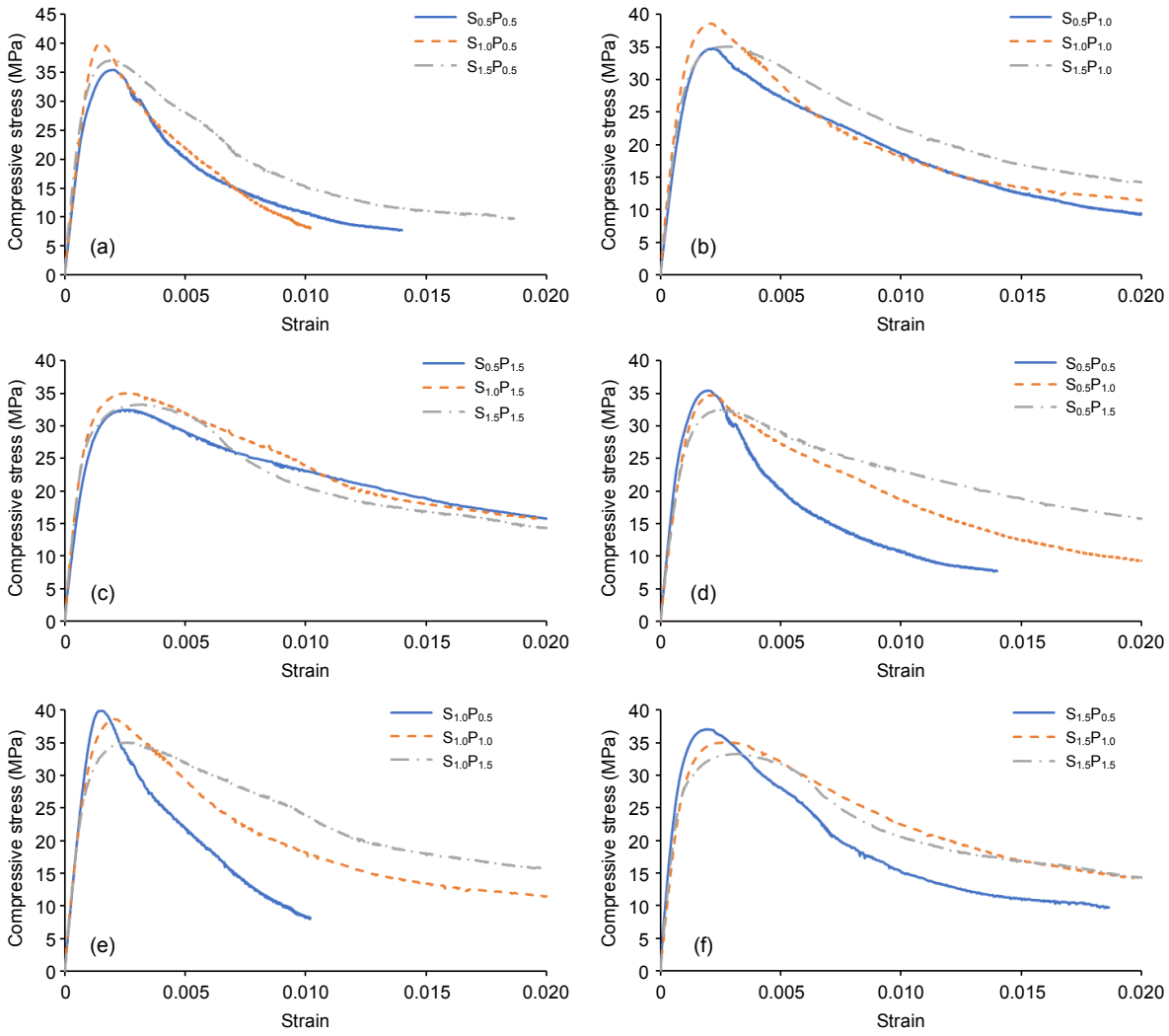

Fig. 2 Compressive stress-strain curves: (a) $S_{0.5}P_{0.5}$, $S_{1.0}P_{0.5}$, and $S_{1.5}P_{0.5}$; (b) $S_{0.5}P_{1.0}$, $S_{1.0}P_{1.0}$, and $S_{1.5}P_{1.0}$; (c) $S_{0.5}P_{1.5}$, $S_{1.0}P_{1.5}$, and $S_{1.5}P_{1.5}$; (d) $S_{0.5}P_{0.5}$, $S_{0.5}P_{1.0}$, and $S_{0.5}P_{1.5}$; (e) $S_{1.0}P_{0.5}$, $S_{1.0}P_{1.0}$, and $S_{1.0}P_{1.5}$; (f) $S_{1.5}P_{0.5}$, $S_{1.5}P_{1.0}$, and $S_{1.5}P_{1.5}$

compressive strength of the steel fiber-reinforced concrete (32.97 MPa) was similar to that of the PVA fiber-reinforced concrete (33.05 MPa). Compared with the single steel fiber-reinforced concrete, HFRC had a higher compressive strength owing to the fiber hybridization effect. However, when the total fiber volume was too high, the compressive strength appeared to decrease. Among all test specimens, the sample with a steel fiber volume of 1.0% and PVA fiber volume of 0.5% had the highest compressive strength, which was 22.3% higher than that of the plain concrete, as the strain corresponding to compressive strength decreased.

Table 1 Compressive test results

Mixture ID	Compressive strength (MPa)	R_t^*	Strain corresponding to compressive strength
$S_{0.5}P_{0.5}$	35.69	1.139	0.00193
$S_{0.5}P_{1.0}$	35.20	1.123	0.00206
$S_{0.5}P_{1.5}$	33.36	1.065	0.00267
$S_{1.0}P_{0.5}$	38.33	1.223	0.00150
$S_{1.0}P_{1.0}$	36.87	1.177	0.00227
$S_{1.0}P_{1.5}$	34.32	1.095	0.00275
$S_{1.5}P_{0.5}$	34.67	1.106	0.00186
$S_{1.5}P_{1.0}$	33.13	1.057	0.00288
$S_{1.5}P_{1.5}$	32.22	1.028	0.00246
$S_{1.0}$	32.97	1.052	0.00223
$P_{1.0}$	33.05	1.055	0.00240
C	31.33	–	0.00181

* R_t is the ratio of the compressive strength of FRC to that of plain concrete (C)

When the steel fiber volume was constant (e.g. at 0.5%, 1.0%, or 1.5%), the compressive strength decreased with increasing PVA fiber volume (Fig. 3b). Taking the samples with a steel fiber volume of 1.0% as an example, the measured compressive strength decreased from 38.33 MPa to 34.32 MPa as the PVA fiber volume increased from 0.5% to 1.5%. In comparison, increasing the steel fiber volume increased the compressive strength when the PVA fiber volume was fixed as a constant value (Fig. 3a). However, when the steel fiber volume was too high (such as above 1.0%), the compressive strength tended to decrease when the steel fiber volume increased. For instance, when the PVA fiber volume was 0.5%, the compressive strength increased by 2.64 MPa as the steel fiber volume increased from 0.5% to 1.0%, but its value decreased by 3.66 MPa when the steel fiber volume continued to increase to 1.5%. We conclude that steel fiber plays a more important role in increasing the compressive strength of HFRC. Zhou et al. (2019) reported a similar phenomenon.

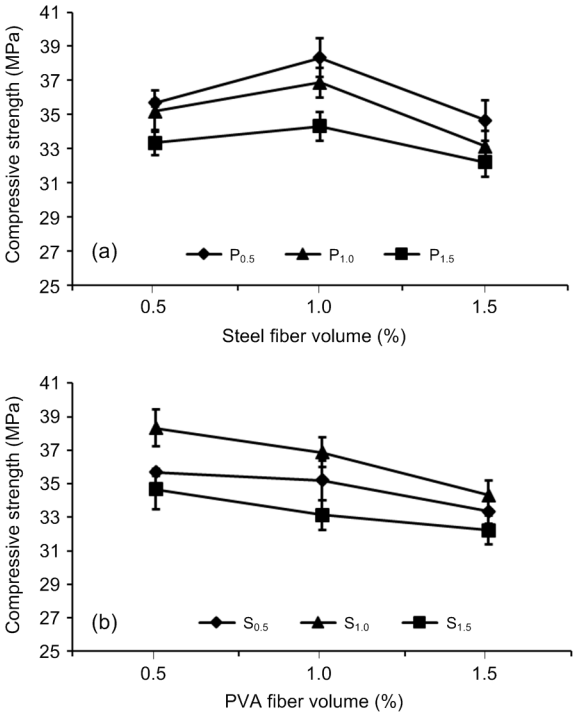

Fig. 3 Effect of fiber type on the compressive strength of HFRC: (a) steel fiber effect; (b) PVA fiber effect

Fig. 4 shows the failure images of HFRC, single fiber-reinforced concrete, and plain concrete during the compressive tests. The plain concrete shows a brittle failure: the width of the crack is large, and a part of the concrete specimen has already spalled (Fig. 4d). The single steel fiber-reinforced concrete (Fig. 4d) shows a relatively small main crack accompanied by little spalling, while there is no obvious spalling in the single PVA fiber-reinforced concrete (Fig. 4d). In comparison, HFRC tends to show a ductile failure rather than a brittle failure; the width of the main crack is smaller and no spalling occurs. When the fiber volume content of steel fibers is constant, adding more PVA fibers reduces the width of the main crack and introduces more noticeable small cracks (Figs. 4a–4c). This is because PVA fibers could improve the tensile behavior of the concrete matrix and consume more energy, delaying the propagation of macrocracks (Liu et al., 2019b, 2020b). During the failure process, the crack seems to be small and short at first, occurring in the middle of the concrete

specimen. With increasing load, more discontinuous and longitudinal short cracks gradually appear and interconnect to generate the main crack. The final failure mode of HFRC is an oblique shear failure. The hybridization effect of steel and PVA fibers might enable HFRC to shift from a brittle to a ductile break (Liu et al., 2019b, 2020a).

Fig. 4 Failure images of HFRC, single fiber-reinforced concrete, and plain concrete: (a) $S_{0.5}P_{0.5}$, $S_{0.5}P_{1.0}$, and $S_{0.5}P_{1.5}$; (b) $S_{1.0}P_{0.5}$, $S_{1.0}P_{1.0}$, and $S_{1.0}P_{1.5}$; (c) $S_{1.5}P_{0.5}$, $S_{1.5}P_{1.0}$, and $S_{1.5}P_{1.5}$; (d) $S_{1.0}$, $P_{1.0}$, and C

3 Relevant data from the literature

The 36 concrete samples tested in this study were insufficient to represent the diversity of HFRC. Therefore, more HFRC data from the literature were collected (Table 2). Although these samples had different cementitious materials, this seems to have had no clear influence on the hybridization of steel and PVA fibers (Liu et al., 2020b). Therefore, all these data, along with those obtained from the above tests were used to prepare the database in this study. Table 3 summarizes the mean, median, and standard deviation of each feature for this database. The size of the whole dataset is 44135. Compared with the compressive stress and the compressive strength, these three indices of the strain corresponding to compressive strength are much lower.

4 Performance of the ANN model

The ANN model that described the compressive behavior was built based on the previous work (Liu et al., 2020a) and its performance was investigated in this section. The details about the ANN model can be found in the electronic supplementary materials. Moreover, a traditional equation-based model was also introduced for comparison with the ANN model. Finally, the performance of the ANN model was discussed.

4.1 Indices for evaluating the model

Apart from the loss function, several different comprehensive indices were used to examine the performance of the ANN model. They included the root mean squared error (RMSE), mean absolute error (MAE), and the coefficient of determination (R^2), which were identified and calculated by Eqs. (1)–(3). The closer R^2 is to 1 and the smaller the values of the other errors, the better the performance of the ANN model.

$$\mathrm{RMSE}(y,\hat{y})=\sqrt{\frac{1}{m}\sum_{i=1}^{m}(y_i-\hat{y}_i)^2}, \tag{1}$$

$$\mathrm{MAE}(y,\hat{y})=\frac{1}{m}\sum_{i=1}^{m}\left|y_i-\hat{y}_i\right|, \tag{2}$$

$$R^2(y,\hat{y})=1-\frac{\sum_{i=1}^{m}(y_i-\hat{y}_i)^2}{\sum_{i=1}^{m}(y_i-\bar{y})^2},\quad \bar{y}=\frac{1}{m}\sum_{i=1}^{m}y_i, \tag{3}$$

where $\hat{y}$ is the predicted value, y is the true value, $\hat{y}_i$ and y_i are the predicted value and the true value of the

Table 2 Steel-PVA fiber hybridization of HFRC from the literature

Cementitious material	Fiber volume (%)		Fiber length (mm)		Fiber diameter (mm)		Number of tested samples	Reference
	Steel fiber	PVA fiber	Steel fiber	PVA fiber	Steel fiber	PVA fiber		
Cement (HFRC)	0.8	0.1	35 or 50	8 or 12	0.55 or 0.75	0.04	16	Zhou et al., 2019
	0.8	0.2						
	1.3	0.1						
	1.3	0.2						
Cement (HFRC)	0.25	0.07	12 or 15	30 or 60	0.5 or 0.73	0.015	16	Yang, 2011
	0.25	0.14						
	0.51	0.07						
	0.51	0.14						
Cement+Fly ash (HFRC)	0.50	0.50	30	12	0.3	0.039	6	Shen, 2013
	0.75	0.75						
Cement (HFRC)	0.50	0.10	30	15	0.5	0.1	3	Arulmurugan, 2018
	0.75	0.25						
	1.00	0.50						

Table 3 Summary of the dataset for the ANN model (size=44 135)

Type	Feature	Mean	Median	Standard deviation
Output	Compressive stress (MPa)	21.48	20.50	10.14
	Compressive strength (MPa)	38.38	37.09	4.89
	Strain corresponding to compressive strength	0.0023	0.0022	0.0005
Input	Strain	0.007 63	0.006 37	0.006 54
	Fiber volume of steel fiber (%)	1.04	1.00	0.37
	Weight of steel fiber (kg)	81.25	78.50	29.18
	Length of steel fiber (mm)	38.89	38.00	4.24
	Diameter of steel fiber (mm)	0.66	0.68	0.06
	Aspect ratio of steel fiber	58.72	56.13	4.07
	Reinforcement index of steel fiber	0.61	0.56	0.22
	Fiber volume of PVA fiber (%)	0.74	0.50	0.52
	Weight of PVA fiber (kg)	9.67	6.50	6.81
	Length of PVA fiber (mm)	11.28	12.00	1.54
	Diameter of PVA fiber (mm)	0.04	0.04	0.00
	Aspect ratio of PVA fiber	287.35	307.69	41.07
	Reinforcement index of PVA fiber	4.00	3.08	6.68
	Elastic modulus of plain concrete (MPa)	36 568.88	36 882.70	1423.41
	Compressive strength of plain concrete (MPa)	34.06	33.05	4.38
	Strain corresponding to compressive strength of plain concrete	0.001 96	0.001 99	0.000 09
	Weight of cement (kg)	291.66	225.00	102.41
	Weight of fly ash (kg)	52.68	75.00	34.29
	Weight of slag powder (kg)	52.68	75.00	34.29
	Weight of water (kg)	176.01	165.00	16.92
	Weight of coarse aggregate (kg)	1018.35	1024.00	8.69
	Weight of fine aggregate (kg)	750.78	785.00	52.58
	Water binder ratio	0.443	0.440	0.005

*i*th sample, respectively, and m is the total number of databases.

4.2 ANN model training and evaluation

The database in Section 3 was used to train and evaluate the ANN model. The loss curves of the training dataset and test dataset are shown in Fig. 5a. Before 480 epochs, the loss values of the training dataset and test dataset varied greatly and showed an obvious decrease. After 480 epochs, the loss values declined gently and tended to converge. This is because the learning parameter was set as 0.01 before 480 epochs and then changed to 0.001. The lowest flat part of the curves can be observed after 960 epochs when the learning rate was changed to 0.0001. The higher learning rate could enable the model to quickly move towards a minimum of the loss function, but would also cause the loss value to oscillate easily, which is suitable for use in the initial stage. By comparison, although a smaller learning rate would slow the forward speed of the model, it could enable the model to converge faster, which is often useful after several epochs.

The RMSE, MAE, and R^2 values of the training and test datasets are shown in Fig. 5b. With the increase in epochs, both the RMSE and MAE of the training and test datasets decreased linearly in the initial stage, then gradually reduced until they converged after 480 epochs. The R^2 of the training and test datasets increased quickly then remained stable after 480 epochs, with both sets having final values above 0.998. All these indices reveal the good performance of the ANN model.

4.3 Equation-based model

For comparison with the ANN model, an equation-based model was also designed based on the constitutive model of MHURD (2011a). The compressive stress-strain curve of HFRC can be described by

$$\sigma = (1-d_c)E_c\varepsilon, \tag{4}$$

$$d_c = \begin{cases} 1-\dfrac{\rho_c n}{n-1+x^n}, & x \le 1, \\ 1-\dfrac{\rho_c}{\alpha_c(x-1)^2+x}, & x > 1, \end{cases} \tag{5}$$

$$\rho_c = \frac{f_{c,r}}{E_c\varepsilon_{c,r}},\ n = \frac{E_c\varepsilon_{c,r}}{E_c\varepsilon_{c,r}-f_{c,r}},\ x = \frac{\varepsilon}{\varepsilon_{c,r}},$$

where σ is the compressive stress; ε is the strain; E_c is the elastic modulus; $f_{c,r}$ is the compressive strength; $\varepsilon_{c,r}$ is the strain corresponding to compressive strength (SCCS); d_c is the damage evolution parameter, which is dependent mainly on the degree of plasticity x, defined as the ratio of ε to $\varepsilon_{c,r}$; α_c is the descending shape parameter, which determines the slope of the descending branch during the post-peak stage; ρ_c, n and x are internal variables. Based on Zhou et al. (2019), the E_c of HFRC was assumed to be identical to that of the corresponding plain concrete in this study.

$f_{c,r}$, $\varepsilon_{c,r}$, and α_c are the main three parameters, and can be determined by back-fitting the experimental data. $f_{c,r}$ and $\varepsilon_{c,r}$ can be easily obtained from the peak value of each compressive stress-strain curve; α_c needs to be calculated by fitting each compressive stress-strain curve using Eq. (5). To describe the effects of steel fiber and PVA fiber, the relationship between these three parameters and the characteristic parameters of steel fiber or PVA fiber need to be formulated. In this study, a polynomial regression was used as a first approximation, as indicated in Eqs. (6)–(8).

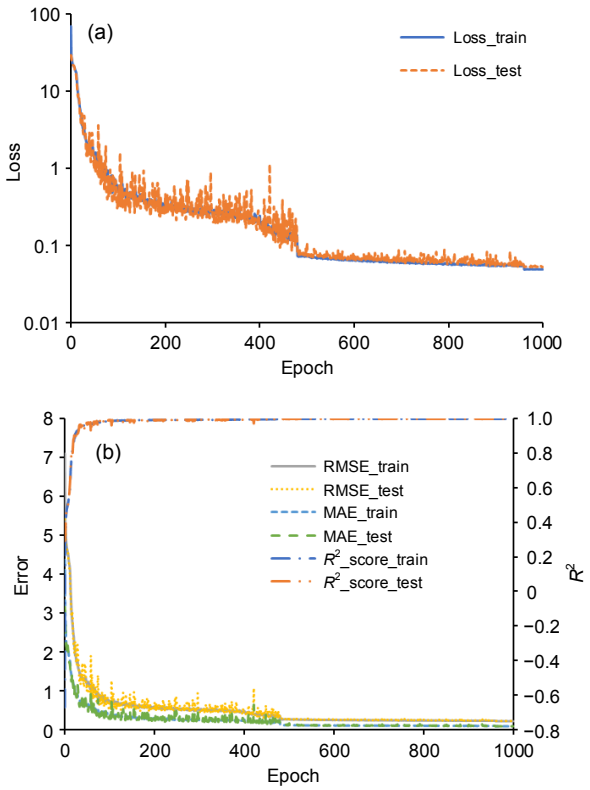

Fig. 5 Training and evaluation results of the ANN model: (a) loss curves; (b) RMSE, MAE, and R^2

$$f_{cH} = f_{cp}(1 + 1.191\lambda_S - 0.091\lambda_P - 0.073\lambda_S\lambda_P - 0.912\lambda_S^2 + 0.017\lambda_P^2), \quad (6)$$

$$\varepsilon_{cH} = \varepsilon_{cp}(1 - 0.967\lambda_S + 0.183\lambda_P + 0.035\lambda_S\lambda_P + 0.891\lambda_S^2 - 0.012\lambda_P^2), \quad (7)$$

$$\alpha_{cH} = (2.720\lambda_S + 0.922\lambda_P - 0.142\lambda_S\lambda_P - 1.334\lambda_S^2 - 0.044\lambda_P^2)^{-1}, \quad (8)$$

$$\lambda_S = \frac{l_S}{d_S}V_S,\ \lambda_P = \frac{l_P}{d_P}V_P,$$

where f_{cH} is the compressive strength of HFRC; ε_{cH} is the SCCS of HFRC; α_{cH} is the descending shape parameter of HFRC; f_{cp} is the compressive strength of plain concrete; ε_{cp} is the SCCS of plain concrete; λ_S is the reinforcement index of steel fibers; λ_P is the reinforcement index of PVA fibers. l_S, d_S, and V_S are the length, diameter, and volume, respectively, of the steel fibers; l_P, d_P, and V_P are the length, diameter, and volume, respectively, of the PVA fibers.

λ_S and λ_P were introduced into Eqs. (6)–(8) to consider the hybridization of steel and PVA fibers because the hybridization effect in HFRC appeared obvious in the above experiments. The back-fitting results are illustrated in Fig. 6. Eqs. (6)–(8) reproduced the trend well, although the value of R^2 was not big.

As indicated in Eq. (6), the addition of PVA fibers decreased the compressive strength of HFRC, while adding a lower volume of steel fibers increased the compressive strength. However, when the fiber volume content of the steel fibers is too high (such as 1.0%), more steel fibers may result in a decrease in the compressive strength. This phenomenon is consistent with the test results in Section 2. Eq. (7) shows that adding both steel and PVA fibers increased the SCCS, and the hybridization of steel and PVA fibers had a positive influence on the SCCS, which is similar to the test results. According to Eq. (8), PVA fibers could significantly influence α_c, reducing the decreasing speed of stress during the post-peak stage.

To describe the compressive stress-strain curve of HFRC, f_{cp}, ε_{cp}, and E_c of the plain concrete were firstly obtained and used as the reference values in Eqs. (6)–(8). Secondly, f_{cH}, ε_{cH}, and α_{cH} were calculated with the fiber information using Eqs. (6)–(8). Then, the compressive stress-strain curve of HFRC was obtained using Eqs. (4) and (5) by replacing $f_{c,r}$, $\varepsilon_{c,r}$, and α_c with these parameters.

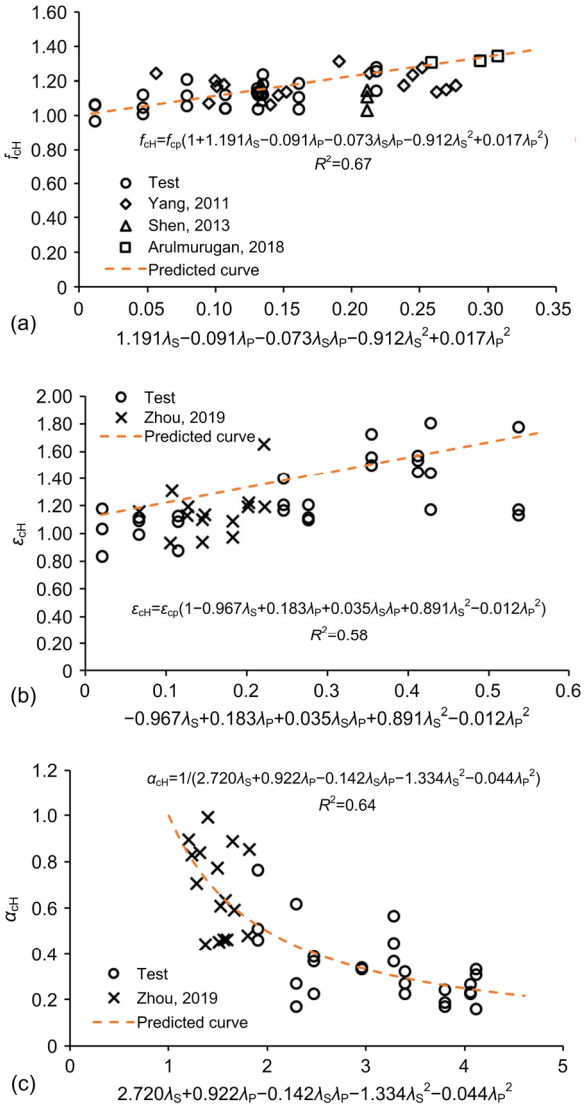

Fig. 6 Back-fitting results of key parameters in the equation-based model: (a) compressive strength, f_{cH}; (b) SCCS, ε_{cH}; (c) descending shape parameter, α_{cH}

4.4 Model performance analysis

Fig. 7 presents the simulation results from the ANN model and the equation-based model, as well as the experimental results of the compressive stress-strain curve of several HFRC samples. Both the ANN model and the equation-based model reproduced the experimental data well, but the ANN model showed a better capacity. For instance, in Fig. 7a, the

equation-based model could predict accurately the stress-strain curve before the peak value, but the difference during the post-peak value increased with the strain. This may be caused by the error of the descending shape parameter induced by Eq. (8); in Fig. 7d, the equation-based predicted compressive stress-strain curve is parallel with the tested curve, owing to the underestimation of the compressive strength by Eq. (6). However, for these two cases, the ANN model reproduced the stress-strain curve well, and almost overlapped the tested curves.

Table 4 summarizes the RMSE, MAE, and R^2 values of the ANN model and the equation-based model. The ANN model had lower errors and a higher R^2 than the equation-based model. Therefore, we conclude that the ANN model can perform better than the equation-based model to reproduce the compressive stress-strain curve.

In this paper, we also introduce the relative error (Zhou et al., 2019) to evaluate the performance of the ANN model and equation-based model in terms of predicting the compressive strength and SCCS. The relative error is calculated by

$$\text{Relative error} = \left|\frac{\text{Predictied value} - \text{Test value}}{\text{Test value}}\right| \times 100\%. \quad (9)$$

Fig. 8 summarizes the relative error obtained using the ANN model and equation-based model. Note that the experimental results are the mean values of different tested specimens with the same fiber content. In terms of compressive strength and SCCS, the predicted value of the ANN model is almost the same as the experimental value. However, obvious relative errors are found for the equation-based model in these two items. This is because of the relatively low value of R^2 when back-fitting Eqs. (6) and (7), as indicated in Fig. 6. The results of this comparison reveal the superior performance of the ANN model for describing the compression behavior of HFRC.

4.5 Sensitivity analysis

Since the ANN model is implicit, it is difficult to understand the relationship between input features and output features. Hence, a sensitivity analysis has been proposed to illustrate how input features affect

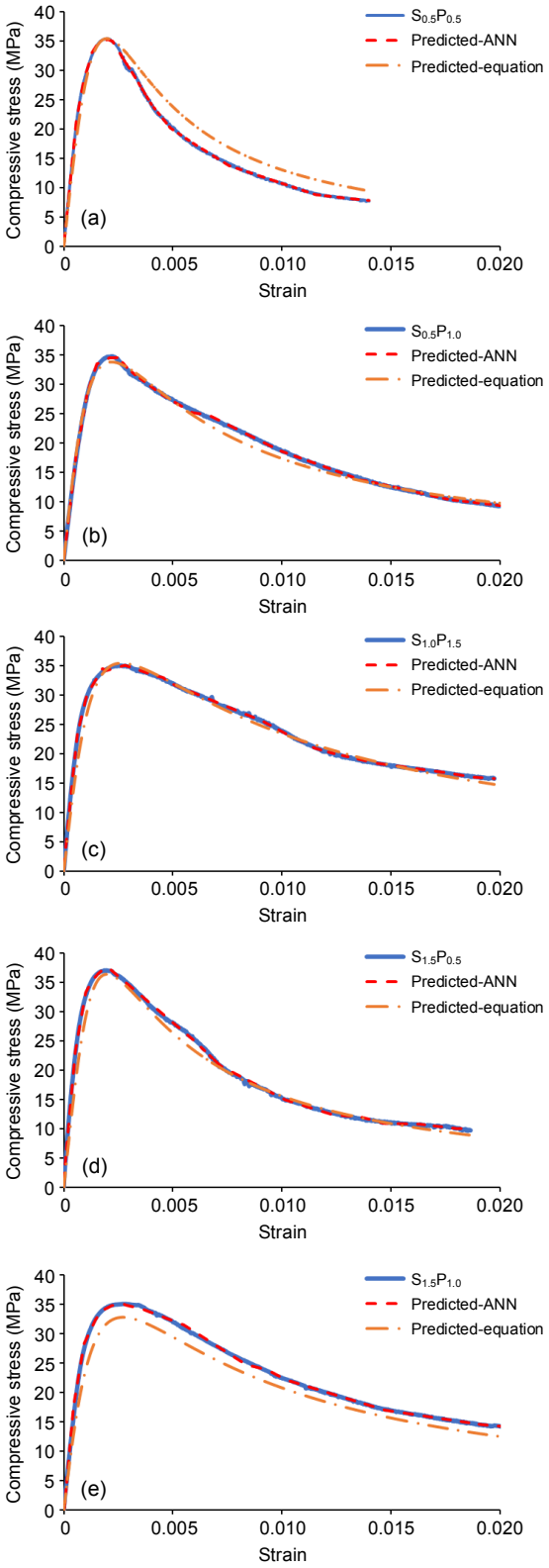

Fig. 7 Comparison of simulation and experimental results of the compressive stress-strain curves: (a) $S_{0.5}P_{0.5}$; (b) $S_{0.5}P_{1.0}$; (c) $S_{1.0}P_{1.5}$; (d) $S_{1.5}P_{0.5}$; (e) $S_{1.5}P_{1.0}$

output features for an ANN model (Saltelli, 2002; Shojaeefard et al., 2013). Among several sensitivity analysis methods, the use of the "PaD" method (partial derivatives) makes it easy to calculate the contribution of each input feature to the specified output feature (Pizarroso et al., 2020).

Fig. 9 shows the contribution of each input feature to the compressive strength and the SCCS for

Table 4 RMSE, MAE, and R^2 of the ANN model and the equation-based model

Mixture ID	RMSE		MAE		R^2	
	ANN	Equation-based	ANN	Equation-based	ANN	Equation-based
$S_{0.5}P_{0.5}$	0.279	2.401	0.218	2.164	0.999	0.939
$S_{0.5}P_{1.0}$	0.238	0.772	0.191	0.616	0.999	0.993
$S_{0.5}P_{1.5}$	0.205	1.723	0.154	1.533	0.999	0.958
$S_{1.0}P_{0.5}$	0.282	2.359	0.210	1.930	0.999	0.933
$S_{1.0}P_{1.0}$	0.301	1.553	0.246	1.207	0.999	0.978
$S_{1.0}P_{1.5}$	0.227	1.296	0.171	0.836	0.999	0.976
$S_{1.5}P_{0.5}$	0.332	1.781	0.247	1.256	0.999	0.966
$S_{1.5}P_{1.0}$	0.389	2.152	0.231	1.975	0.998	0.936
$S_{1.5}P_{1.5}$	0.241	2.556	0.154	2.027	0.999	0.895

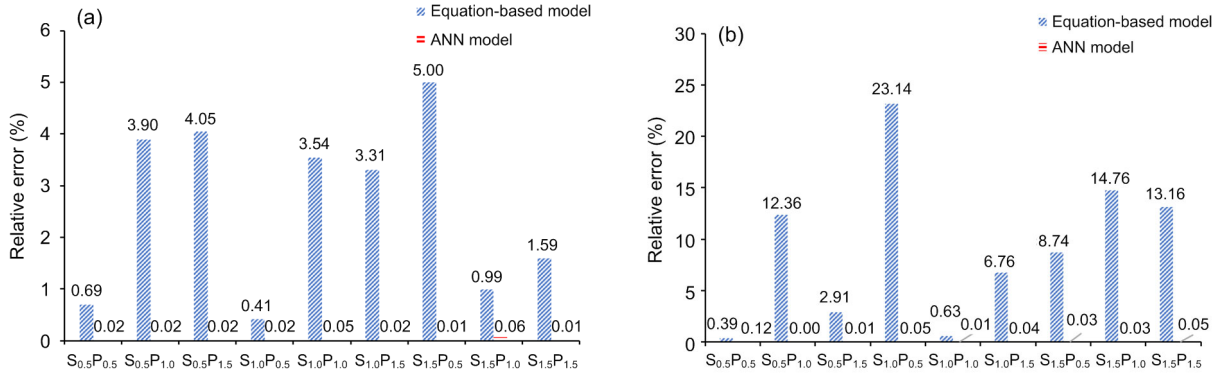

Fig. 8 Relative errors of the ANN model and the equation-based model in terms of the compressive strength (a) and SCCS (b)

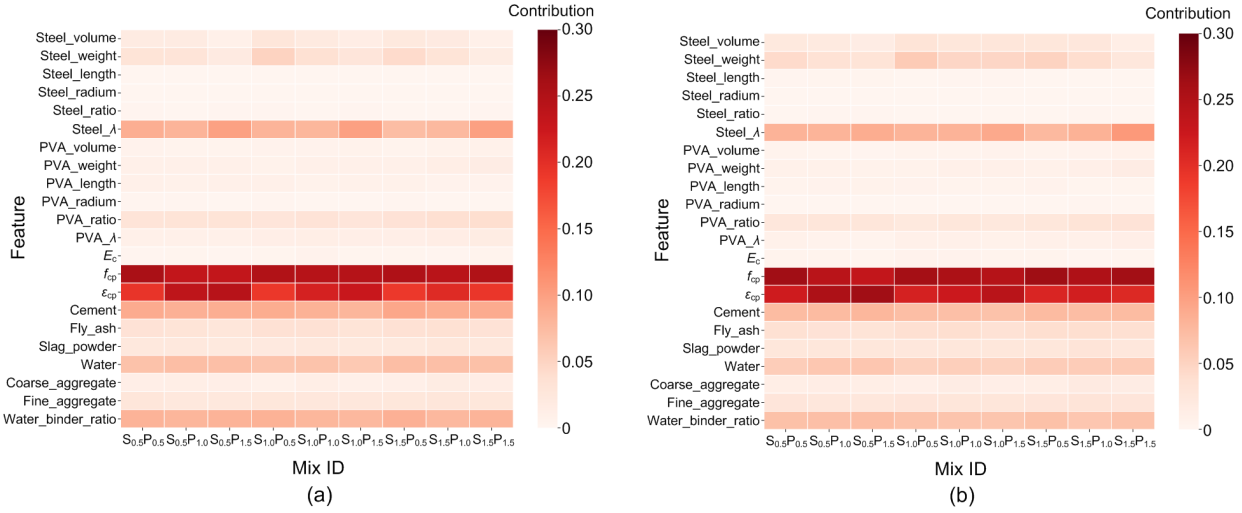

Fig. 9 Contributions of each input feature to the compressive strength (a) and the strain corresponding to compressive strength of HFRC (b)

HFRC samples. The redder the color, the higher the contribution of the specified input feature. The highest contribution appears to be the compressive strength and the SCCS of plain concrete. There are four main influence parts, including steel fibers, PVA fibers, mechanical properties of plain concrete, and components of HFRC. Fig. 10 reveals the contribution of these four main parts to the compressive strength and the SCCS, which is the sum of their sub-input features. According to Figs. 9 and 10, the mechanical properties of plain concrete make the main contribution to the compressive strength and the SCCS for all HFRC samples. The contribution of steel fibers is higher than that of PVA fibers in terms of the compressive strength and the SCCS for all HFRC samples. This is similar to the experimental results.

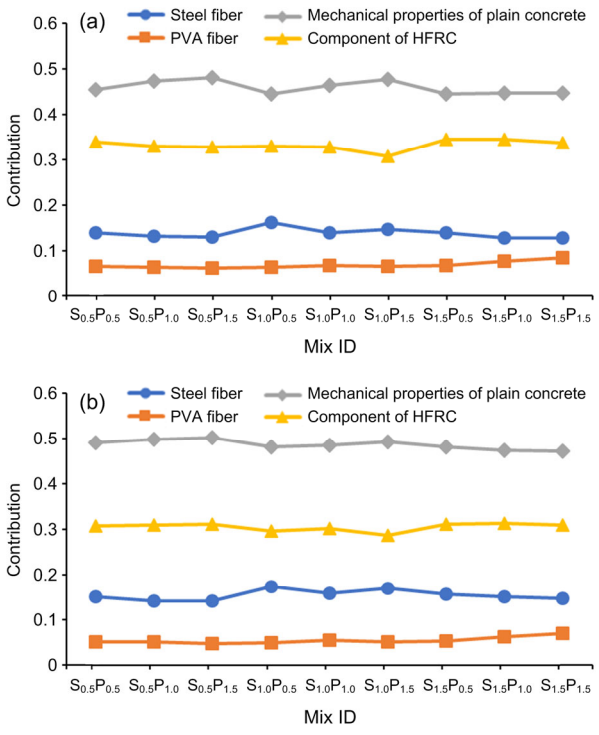

Fig. 10 Contribution of steel fibers, PVA fibers, mechanical properties of plain concrete, and components of HFRC to the compressive strength (a) and the SCCS (b)

4.6 Discussion

According to the analysis above, it is clear that the ANN model developed in this study is better able to describe the compressive behavior of HFRC than the equation-based model. The performance of the equation-based model depends on the determination of key parameters, including the compressive strength, SCCS, and descending shape parameter, calculated using Eqs. (6)–(8). If one of these parameters is not well determined, the predicted compressive stress-strain curve would not fit well with the experimental results. Also, only limited factors are considered in Eqs. (6)–(8), and many other components, such as the cementitious material, that could significantly influence the mechanical properties of concrete, are not directly considered in these equations. The R^2 value of Eqs. (6)–(8) seems relatively low, indicating that the equation-based model could reproduce well the stress-strain curve for some HFRC samples while having obvious error for others, as shown in Figs. 6 and 7. However, the equation-based model is simple and can be easily used in the calculation of the structural components and structures, resulting in the wide application of such types of models. In summary, the equation-based model needs further development, especially the methodology to consider the effects of different compositions.

By comparison, the ANN model can consider more factors. Thus, it is able to extract more important features and has more powerful nonlinear fitting abilities, resulting in a better capacity to predict the compressive stress-strain curve of HFRC. Moreover, the ANN model could be applied not only to HFRC, but also to other composite materials (such as ultra-high-performance concrete) and even material that contains different composite components, which are difficult to model by an equation-based model. On the other hand, the ANN model needs a large database to improve its performance, especially when it is used to predict the stress-strain curve. To consider these factors, more and credible databases are necessary, and this work is being carried out by our group. Furthermore, the geometry of steel fibers and PVA fibers may also affect the compressive behavior, but cannot be considered by the current ANN model. However, the influence of these factors could be clarified via the ANN model when the diversity of the database is big enough. Also, the training of the ANN model needs time. For example, about 1 h was necessary for training the ANN model in this study based on GeForce RTX 2070 SUPER GPU. When adding more datasets, the model needs a longer time for training to

improve its performance. However, these problems may be solved by developments in computer science. As a first approximation, the presented work demonstrates the suitability of the ANN model for describing the compressive behavior of HFRC.

In summary, the choice of an equation-based model or an ANN model should be related to actual needs. The ANN model is more suitable for the accurate design of composite material, such as HFRC, while the equation-based model can be easily used in structural analysis.

5 Conclusions

This paper presents a comprehensive investigation on the compressive behavior of HRFC containing fly ash and slag powder via experiments and modelling. A series of experiments were carried out to investigate the hybrid effect of steel and PVA fiber on the compressive behavior of HFRC containing fly ash and slag powder. Meanwhile, an ANN model to describe the compressive behavior was also built and trained with the experimental data and relevant data from the literature. The performance of the ANN model was compared to an equation-based model. Based on the above work, the following conclusions can be drawn:

1. The proposed ANN model has a better capacity than the equation-based model to reproduce the compressive behavior of hybrid steel-PVA fiber concrete containing fly ash and slag powder in terms of the compressive stress-strain curve, the compressive strength, and the SCCS. The ANN model can consider many factors affecting the mechanical behavior of HFRC. In this study, 23 factors were considered, including features of fibers, concrete composition, and mechanical behavior of plain concrete. Note that more factors may be included when the database is large enough. Therefore, the ANN model is a good tool for designing composite materials, and is not limited to HFRC.

2. Both the experimental results and the ANN model simulation results revealed that steel fibers play a more important role in increasing the compressive strength of HFRC than PVA fibers, while both contribute to the deformation. Increasing the steel fiber volume could increase the compressive strength, while increasing the PVA fiber volume could reduce it. However, when the steel fiber volume is too high (such as above 1.0%), the compressive strength tends to decrease with increasing steel fiber volume. The hybridization effect of steel and PVA fibers could enable HFRC to shift from a brittle break to a ductile break.

Contributors

Fang-yu LIU, Wen-qi DING, and Ya-fei QIAO designed the research. Fang-yu LIU, Ya-fei QIAO, and Qi-yang CHEN processed the corresponding data. Fang-yu LIU and Ya-fei QIAO wrote the first draft of the manuscript. Wen-qi DING and Lin-bing WANG helped to organize the manuscript. Fang-yu LIU, Wen-qi DING, Ya-fei QIAO, and Lin-bing WANG revised and edited the final version.

Conflict of interest

Fang-yu LIU, Wen-qi DING, Ya-fei QIAO, Lin-bing WANG, and Qi-yang CHEN declare that they have no conflict of interest.

References

Açikgenç M, Ulaş M, Alyamaç KE, 2015. Using an artificial neural network to predict mix compositions of steel fiber-reinforced concrete. *Arabian Journal for Science and Engineering*, 40(2):407-419. https://doi.org/10.1007/s13369-014-1549-x

Arulmurugan P, 2018. Evaluation of FRC beams using steel and pva fibres in concrete. *International Journal of Advance Research and Innovation*, 6(1):121-124.

Bai J, Wild S, Ware JA, et al., 2003. Using neural networks to predict workability of concrete incorporating metakaolin and fly ash. *Advances in Engineering Software*, 34(11-12): 663-669. https://doi.org/10.1016/S0965-9978(03)00102-9

Belletti B, Cerioni R, Meda A, et al., 2008. Design aspects on steel fiber-reinforced concrete pavements. *Journal of Materials in Civil Engineering*, 20(9):599-607. https://doi.org/10.1061/(asce)0899-1561(2008)20:9(599)

Blanco A, Pujadas P, de la Fuente A, et al., 2016. Influence of the type of fiber on the structural response and design of FRC slabs. *Journal of Structural Engineering*, 142(9): 04016054. https://doi.org/10.1061/(ASCE)ST.1943-541X.0001515

CAECS (China Association for Engineering Construction Standardization), 2010. Standard Test Methods for Fiber Reinforced Concrete, CECS 13:2009. National Standards of the People's Republic of China (in Chinese).

Chi Y, Xu LH, Yu HS, 2014a. Constitutive modeling of steel-polypropylene hybrid fiber reinforced concrete using a non-associated plasticity and its numerical implementation. *Composite Structures*, 111:497-509. https://doi.org/10.1016/j.compstruct.2014.01.025

Chi Y, Xu LH, Zhang YY, 2014b. Experimental study on hybrid fiber-reinforced concrete subjected to uniaxial compression. *Journal of Materials in Civil Engineering*, 26(2):211-218. https://doi.org/10.1061/(ASCE)MT.1943-5533.0000764

de la Fuente A, Pujadas P, Blanco A, et al., 2012. Experiences in Barcelona with the use of fibres in segmental linings. *Tunnelling and Underground Space Technology*, 27(1): 60-71. https://doi.org/10.1016/j.tust.2011.07.001

Ding WQ, Gong YF, Qiao YF, et al., 2020. Experimental investigation on mechanical behavior of segmental joint under combined loading of compression-bending-shear. *Tunnelling and Underground Space Technology*, 98: 103346. https://doi.org/10.1016/j.tust.2020.103346

Feng J, Sun WW, Zhai HZ, et al., 2018. Experimental study on hybrid effect evaluation of fiber reinforced concrete subjected to drop weight impacts. *Materials*, 11(12): 2563. https://doi.org/10.3390/ma11122563

Gong CJ, Ding WQ, Mosalam KM, et al., 2017. Comparison of the structural behavior of reinforced concrete and steel fiber reinforced concrete tunnel segmental joints. *Tunnelling and Underground Space Technology*, 68: 38-57. https://doi.org/10.1016/j.tust.2017.05.010

Hai R, Liu JX, Zhang ML, et al., 2016. Performance of hybrid steel-polyvinyl alcohol fiber reinforced ultra high performance concrete. *Concrete*, (5):95-97 (in Chinese). https://doi.org/10.3969/j.issn.1002-3550.2016.05.025

Hossain KMA, Lachemi M, Sammour M, et al., 2013. Strength and fracture energy characteristics of self-consolidating concrete incorporating polyvinyl alcohol, steel and hybrid fibres. *Construction and Building Materials*, 45:20-29. https://doi.org/10.1016/j.conbuildmat.2013.03.054

Jiang KJ, Han Q, Bai YL, et al., 2020. Data-driven ultimate conditions prediction and stress-strain model for FRP-confined concrete. *Composite Structures*, 242:112094. https://doi.org/10.1016/j.compstruct.2020.112094

Karahan O, Tanyildizi H, Atis CD, 2008. An artificial neural network approach for prediction of long-term strength properties of steel fiber reinforced concrete containing fly ash. *Journal of Zhejiang University-SCIECNE A*, 9:1514-1523. https://doi.org/10.1631/jzus.A0720136

Lawler JS, Wilhelm T, Zampini D, et al., 2003. Fracture processes of hybrid fiber-reinforced mortar. *Materials and Structures*, 36(3):197-208. https://doi.org/10.1007/BF02479558

Lawler JS, Zampini D, Shah SP, 2005. Microfiber and macrofiber hybrid fiber-reinforced concrete. *Journal of Materials in Civil Engineering*, 17(5):595-604. https://doi.org/10.1061/(asce)0899-1561(2005)17:5(595)

Li HY, Liu G, 2016. Tensile properties of hybrid fiber-reinforced reactive powder concrete after exposure to elevated temperatures. *International Journal of Concrete Structures and Materials*, 10(1):29-37. https://doi.org/10.1007/s40069-016-0125-z

Liao L, de la Fuente A, Cavalaro S, et al., 2015. Experimental and analytical study of concrete blocks subjected to concentrated loads with an application to TBM-constructed tunnels. *Tunnelling and Underground Space Technology*, 49:295-306. https://doi.org/10.1016/j.tust.2015.04.020

Liu FY, Ding WQ, Qiao YF, 2019a. An experimental investigation on the integral waterproofing capacity of polypropylene fiber concrete with fly ash and slag powder. *Construction and Building Materials*, 212:675-686. https://doi.org/10.1016/j.conbuildmat.2019.04.027

Liu FY, Ding WQ, Qiao YF, 2019b. Experimental investigation on the flexural behavior of hybrid steel-PVA fiber reinforced concrete containing fly ash and slag powder. *Construction and Building Materials*, 228:116706. https://doi.org/10.1016/j.conbuildmat.2019.116706

Liu FY, Ding WQ, Qiao YF, et al., 2020a. An artificial neural network model on tensile behavior of hybrid steel-PVA fiber reinforced concrete containing fly ash and slag power. *Frontiers of Structural and Civil Engineering*, 14: 1299-1315. https://doi.org/10.1007/s11709-020-0712-6

Liu FY, Ding WQ, Qiao YF, 2020b. Experimental investigation on the tensile behavior of hybrid steel-PVA fiber reinforced concrete containing fly ash and slag powder. *Construction and Building Materials*, 241:118000. https://doi.org/10.1016/j.conbuildmat.2020.118000

Mashhadban H, Kutanaei SS, Sayarinejad MA, 2016. Prediction and modeling of mechanical properties in fiber reinforced self-compacting concrete using particle swarm optimization algorithm and artificial neural network. *Construction and Building Materials*, 119:277-287. https://doi.org/10.1016/j.conbuildmat.2016.05.034

MHURD (Ministry of Housing and Urban-Rural Development of the People's Republic of China), 2011a. Code for Design of Concrete Structure, GB 50010-2010. National Standards of People's Republic of China (in Chinese).

MHURD (Ministry of Housing and Urban-Rural Development of the People's the Republic of China), 2011b. Specification for Mix Proportion Design of Ordinary Concrete, JGJ 55-2011. National Standards of the People's Republic of China (in Chinese).

Nguyen DL, Kim DJ, Ryu GS, et al., 2013. Size effect on flexural behavior of ultra-high-performance hybrid fiber-reinforced concrete. *Composites Part B: Engineering*, 45(1):1104-1116. https://doi.org/10.1016/j.compositesb.2012.07.012

Pizarroso J, Portela J, Muñoz A, 2020. NeuralSens: sensitivity analysis of neural networks. arXiv: 2002.11423. https://arxiv.org/abs/2002.11423

Pujadas P, Blanco A, Cavalaro S, et al., 2014. Plastic fibres as the only reinforcement for flat suspended slabs: experimental investigation and numerical simulation.

Construction and Building Materials, 57:92-104. https://doi.org/10.1016/j.conbuildmat.2014.01.082

Pujadas P, Blanco A, Cavalaro S, et al., 2017. The need to consider flexural post-cracking creep behavior of macro-synthetic fiber reinforced concrete. *Construction and Building Materials*, 149:790-800. https://doi.org/10.1016/j.conbuildmat.2017.05.166

Saltelli A, 2002. Sensitivity analysis for importance assessment. *Risk Analysis*, 22(3):579-590. https://doi.org/10.1111/0272-4332.00040

Serna Ros P, Martí-Vargas JR, Bossio ME, et al., 2016. Creep and residual properties of cracked macro-synthetic fibre reinforced concretes. *Magazine of Concrete Research*, 68(4):197-207. https://doi.org/10.1680/macr.15.00111

Shen QZ, 2013. Mechanical Properties Research for Steel-PVA Hybrid Fibers Reinforced Concrete. MS Thesis, Chang'an University, Xi'an, China (in Chinese).

Shojaeefard MH, Akbari M, Tahani M, et al., 2013. Sensitivity analysis of the artificial neural network outputs in friction stir lap joining of aluminum to brass. *Advances in Materials Science and Engineering*, 2013:574914. https://doi.org/10.1155/2013/574914

Sim JS, Park C, Moon DY, 2005. Characteristics of basalt fiber as a strengthening material for concrete structures. *Composites Part B: Engineering*, 36(6-7):504-512. https://doi.org/10.1016/j.compositesb.2005.02.002

Soutsos MN, Le TT, Lampropoulos AP, 2012. Flexural performance of fibre reinforced concrete made with steel and synthetic fibres. *Construction and Building Materials*, 36:704-710. https://doi.org/10.1016/j.conbuildmat.2012.06.042

Stoll F, Saliba JE, Casper LE, 2000. Experimental study of CFRP-prestressed high-strength concrete bridge beams. *Composite Structures*, 49(2):191-200. https://doi.org/10.1016/S0263-8223(99)00134-8

Tabatabaeian M, Khaloo A, Joshaghani A, et al., 2017. Experimental investigation on effects of hybrid fibers on rheological, mechanical, and durability properties of high-strength SCC. *Construction and Building Materials*, 147:497-509. https://doi.org/10.1016/j.conbuildmat.2017.04.181

Xu LH, Xu HR, Chi Y, et al., 2011. Experimental study on tensile strength of steel-polypropylene hybrid fiber reinforced concrete. *Advanced Science Letters*, 4(3):911-916. https://doi.org/10.1166/asl.2011.1740

Yang KH, 2011. Tests on concrete reinforced with hybrid or monolithic steel and polyvinyl alcohol fibers. *ACI Materials Journal*, 108(6):664-672.

Zhao GY, di Prisco M, Vandewalle L, 2015. Experimental investigation on uniaxial tensile creep behavior of cracked steel fiber reinforced concrete. *Materials and Structures*, 48(10):3173-3185. https://doi.org/10.1617/s11527-014-0389-1

Zhou Y, Xiao Y, Gu AQ, et al., 2018. Dispersion, workability and mechanical properties of different steel-microfiber-reinforced concretes with low fiber content. *Sustainability*, 10(7):2335. https://doi.org/10.3390/su10072335

Zhou Y, Xiao Y, Gu AQ, et al., 2019. Orthogonal experimental investigation of steel-PVA fiber-reinforced concrete and its uniaxial constitutive model. *Construction and Building Materials*, 197:615-625. https://doi.org/10.1016/j.conbuildmat.2018.11.203

List of electronic supplementary materials

Data S1 Framework of the ANN model